International Conference on Mathematics, Computational Methods & Reactor Physics (M&C 2009)
Saratoga Springs, New York, May 3-7, 2009, on CD-ROM, American Nuclear Society, LaGrange Park, IL (2009)

SWEEPLESS TIME-DEPENDENT TRANSPORT SIMULATIONS USING THE STAGGERED-BLOCK JACOBI METHOD

G. Davidson and E.W. Larsen
University of Michigan
2355 Bonisteel Boulevard
Ann Arbor, MI 48109
davidsgr@umich.edu; edlarsen@umich.edu

ABSTRACT

The Staggered-Block Jacobi (SBJ) method is a new numerical S_N transport method for solving time-dependent problems without sweeps or low-order acceleration. Because it is a Jacobian method, it is trivial to parallelize and will scale linearly with the number of processors. It is highly accurate in thick-diffusive problems and unconditionally stable when combined with the lumped linear discontinuous finite element spatial discretization. In this way, the SBJ method is complementary to sweep-based methods, which are accurate and efficient in thin, streaming regions but inefficient in thick, diffusive problems without acceleration. We have extended previous work by demonstrating how sweep-based methods and the SBJ method may be combined to produce a method which is accurate and efficient without acceleration in all optical thicknesses while still retaining good parallel efficiency. Furthermore, iterations may also be added to the SBJ method. This is particularly useful for improving the accuracy of the SBJ method in intermediate-thickness problems.

Key Words: transport, jacobi, time-dependent

1. INTRODUCTION

Currently, time-dependent transport problems are simulated by discretizing in time and solving a steady-state transport problem within each time step; the steady-state problem is solved using transport sweeps, and if necessary, low-order acceleration. In this paper we present a new method for solving time-dependent transport problems in which sweeps are not required. This method is complementary to sweep-based methods in that it is optimal for optically thick media, and is easily parallelizable. Previous work on sweepless transport methods was performed by Klar [1],[2], whose method was limited to thick diffusive regimes and, unlike the method presented here, was not unconditionally stable. This paper continues and expands the work presented in Ref. [3].

2. THE STAGGERED-BLOCK JACOBI EQUATIONS

2.1. Deriving the Staggered-Block Jacobi Equations

In the present work we consider the one-dimensional, energy-independent transport equation with the lumped linear-discontinuous (LD) finite element spatial discretization [4] and the discrete ordinates angular discretization [5]. Under these conditions, there are two unknowns for each angle

in each cell. We will begin our derivation with the implicitly time-differenced (backwards-Euler) fully-lumped finite-element transport equation for a cell i:

$$\frac{1}{v\Delta t_{k+1}}\underline{\underline{M}}_i\left(\underline{\psi}_{n,i}^{k+1}-\underline{\psi}_{n,i}^{k}\right)+\mu_n\underline{\underline{L}}_i^{surf}\underline{\psi}_{n,i}^{k+1,surf}-\mu_n\underline{\underline{L}}_i\underline{\psi}_{n,i}^{k+1}+\Sigma_{t,i}\underline{\underline{M}}_i\underline{\psi}_{n,i}^{k+1}$$
$$=\frac{\Sigma_{s,i}}{2}\underline{\underline{M}}_i\sum_{m=1}^{N}\underline{\psi}_{m,i}^{k+1}\Delta_m+\underline{\underline{M}}_i\underline{Q}_{n,i}^{k+1}\,. \quad (1)$$

This equation is similar to the lumped finite-element equation given in [4], with two exceptions. First, our equation is time-dependent, so a time derivative (the first term) is added. Second, we define our leakage matrix $\underline{\underline{L}}_i$ to have the opposite sign as Adams, i.e.,

$$\underline{\underline{L}}_i=\begin{bmatrix}-\frac{1}{2} & -\frac{1}{2}\\ \frac{1}{2} & \frac{1}{2}\end{bmatrix}\,. \quad (2)$$

All of our matrices are lumped, so we have omitted the *lump* superscripts that are present on the matrices in [4]. The other quantities are defined as follows:

$$v=\text{particle speed}\,, \quad (3a)$$

$$\Delta t_{k+1}=\text{length of time step } k+1\,, \quad (3b)$$

$$\mu_n=\text{cosine of angle between particle flight direction and } x\text{-axis}\,, \quad (3c)$$

$$\Sigma_{t,i}=\text{total cross section in cell } i\,, \quad (3d)$$

$$\Sigma_{s,i}=\text{scattering cross section in cell } i\,, \quad (3e)$$

$$\underline{\psi}_{n,i}^{k+1}=\begin{bmatrix}\psi_{n,i,L}^{k+1}\\ \psi_{n,i,R}^{k+1}\end{bmatrix}\,, \quad (3f)$$

$$\underline{\psi}_{n,i}^{k+1,surf}=\begin{bmatrix}\psi_{n,i,R}^{k+1,surf}\\ \psi_{n,i,R}^{k+1,surf}\end{bmatrix}\,, \quad (3g)$$

$$\underline{Q}_{n,i}^{k+1}=\begin{bmatrix}Q_{n,i,L}^{k+1}\\ Q_{n,i,R}^{k+1}\end{bmatrix}\,. \quad (3h)$$

The quantities $\psi_{n,i,L}^{k+1}$ and $\psi_{n,i,R}^{k+1}$ represent the angular fluxes on the left and right sides of cell i at angular ordinate n and time $k+1$, respectively. Likewise, the quantities $Q_{n,i,L}^{k+1}$ and $Q_{n,i,R}^{k+1}$ represent a particle source on the left and right sides of cell i at angular ordinate n and time $k+1$. The quantities $\psi_{n,i,L}^{k+1,surf}$ and $\psi_{n,i,R}^{k+1,surf}$ represent the angular fluxes on the left and right surfaces of cell i, and are closed with the standard upstream closure. For $\mu_n<0$ we have

$$\psi_{n,i,L}^{k+1,surf}=\psi_{n,i,L}^{k+1}\,, \quad (4a)$$

$$\psi_{n,i,R}^{k+1,surf} = \begin{cases} \psi_{n,i+1,L}^{k+1}\,, & 1 \le i \le I-1\,, \\ \psi_{n,R}^{b,k+1}\,, & i = I\,, \end{cases} \tag{4b}$$

and for $\mu_n > 0$ we have

$$\psi_{n,i,L}^{k+1,surf} = \begin{cases} \psi_{n,L}^{b,k+1}\,, & i = 1\,, \\ \psi_{n,i-1,R}^{k+1}\,, & 2 \le i \le I\,, \end{cases} \tag{5a}$$

$$\psi_{n,i,R}^{k+1,surf} = \psi_{n,i,R}^{k+1}\,, \tag{5b}$$

where $\psi_{n,L}^{b,k+1}$ and $\psi_{n,R}^{b,k+1}$ represent the incident angular flux in angular ordinate n for time $k+1$ for the right and left boundaries, respectively. The lumped linear-discontinuous finite element matrices are defined as

$$\underline{\underline{M}}_i = \frac{\Delta x_i}{2}\begin{bmatrix} 1 & 0 \\ 0 & 1 \end{bmatrix}\,, \qquad \text{Mass Matrix}\,, \tag{6a}$$

$$\underline{\underline{L}}_i^{surf} = \begin{bmatrix} -1 & 0 \\ 0 & 1 \end{bmatrix}\,. \tag{6b}$$

These implicitly-differenced finite-element equations are solved by guessing the scattering source and sweeping across the mesh in each angular direction. After every angular direction has been swept, the scattering source is updated, and the process is repeated until the iterations converge. This is called source iteration, and for thick, diffusive problems can converge arbitrarily slowly. Typically, diffusion synthetic acceleration [6] and sometimes Krylov solvers [7] are employed to converge the scattering source more quickly.

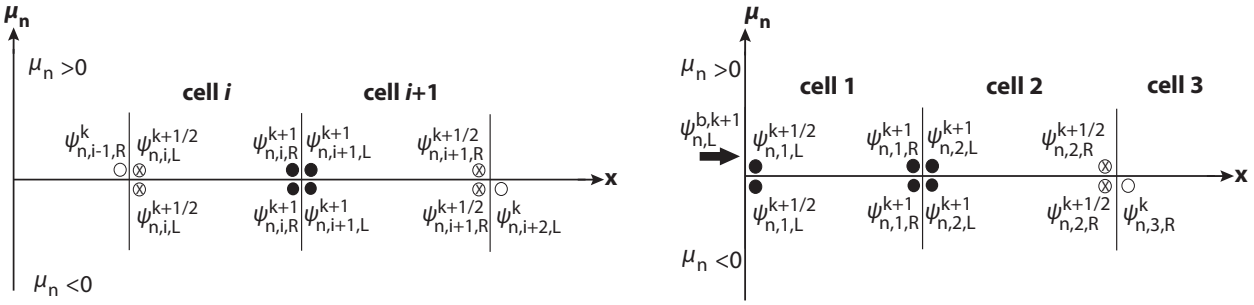

Figure 1. SBJ Space-Time Stencil for the Interior (*left*) and Left Boundary (*right*)

The concept behind the staggered block Jacobi (SBJ) method is as follows: consider a *block* of two cells, i and $i+1$. The incident flux on the block boundary is evaluated at time k. The unknown fluxes inside the two-cell block are obtained by solving the full S_N equations for the two cells, with the specified incident fluxes at time k. The flux unknowns located adjacent to the interior zone-boundary (see Figure 1, *left*) are evaluated at time $k+1$. The angular flux unknowns located at the edges of the blocks (labeled with time $k+1/2$ in Figure 1, *left*) are discarded. The equations

for the SBJ method in the domain interior are

$$\frac{1}{v\Delta t_{k+1}}\underline{\underline{\hat{M}}}_{i+1/2}\left(\underline{\psi}^{k+1,\textit{SBJ}}_{n,i+1/2}-\underline{\psi}^{k}_{n,i+1/2}\right)+\mu_n\underline{\underline{\hat{L}}}^{\textit{surf}}_{i+1/2}\underline{\psi}^{k,\textit{surf}}_{n,i+1/2}-\mu_n\underline{\underline{\hat{L}}}_{i+1/2}\underline{\psi}^{k+1,\textit{SBJ}}_{n,i+1/2}+\underline{\underline{\hat{T}}}_{i+1/2}\underline{\psi}^{k+1,\textit{SBJ}}_{n,i+1/2}$$
$$=\frac{1}{2}\underline{\underline{\hat{S}}}_{i+1/2}\sum_{m=1}^{N}\underline{\psi}^{k+1,\textit{SBJ}}_{n,i+1/2}\Delta_m+\underline{\underline{\hat{M}}}_{i+1/2}\underline{Q}^{k+1}_{n,i+1/2}\,, \quad (7)$$

where

$$\underline{\psi}^{k+1,\textit{SBJ}}_{n,i+1/2}=\begin{bmatrix}\psi^{k+1/2}_{n,i,L}\\ \psi^{k+1}_{n,i,R}\\ \psi^{k+1}_{n,i+1,L}\\ \psi^{k+1/2}_{n,i+1,R}\end{bmatrix}, \quad (8a)$$

$$\underline{\psi}^{k}_{n,i+1/2}=\begin{bmatrix}\psi^{k}_{n,i,L}\\ \psi^{k}_{n,i,R}\\ \psi^{k}_{n,i+1,L}\\ \psi^{k}_{n,i+1,R}\end{bmatrix}, \quad (8b)$$

$$\underline{Q}^{k+1}_{n,i+1/2}=\begin{bmatrix}Q^{k+1}_{n,i,L}\\ Q^{k+1}_{n,i,R}\\ Q^{k+1}_{n,i+1,L}\\ Q^{k+1}_{n,i+1,R}\end{bmatrix}, \quad (8c)$$

and

$$\underline{\psi}^{k,\textit{surf}}_{n,i+1/2}=\begin{bmatrix}\psi^{k}_{n,i,L}\\ \psi^{k+1}_{n,i,R}\\ \psi^{k+1}_{n,i+1,L}\\ \psi^{k+1/2}_{n,i+1,R}\end{bmatrix}, \qquad \mu_n>0\,, \quad (9a)$$

$$\underline{\psi}^{k,\textit{surf}}_{n,i+1/2}=\begin{bmatrix}\psi^{k+1/2}_{n,i,L}\\ \psi^{k+1}_{n,i,R}\\ \psi^{k+1}_{n,i+1,L}\\ \psi^{k}_{n,i+1,R}\end{bmatrix}, \qquad \mu_n<0\,, \quad (9b)$$

and where the 4×4 matrices are defined as

$$\underline{\underline{\hat{M}}}_{i+1/2}=\begin{bmatrix}\underline{\underline{M}}_i & \underline{\underline{0}}\\ \underline{\underline{0}} & \underline{\underline{M}}_{i+1}\end{bmatrix}, \quad (10a)$$

$$\underline{\underline{\hat{T}}}_{i+1/2} = \begin{bmatrix} \Sigma_{t,i}\underline{\underline{M}}_i & \underline{\underline{0}} \\ \underline{\underline{0}} & \Sigma_{t,i+1}\underline{\underline{M}}_{i+1} \end{bmatrix}, \tag{10b}$$

$$\underline{\underline{\hat{S}}}_{i+1/2} = \begin{bmatrix} \Sigma_{s,i}\underline{\underline{M}}_i & \underline{\underline{0}} \\ \underline{\underline{0}} & \Sigma_{s,i+1}\underline{\underline{M}}_{i+1} \end{bmatrix}, \tag{10c}$$

$$\underline{\underline{\hat{L}}}^{surf}_{i+1/2} = \begin{bmatrix} \underline{\underline{L}}^{surf}_i & \underline{\underline{0}} \\ \underline{\underline{0}} & \underline{\underline{L}}^{surf}_{i+1} \end{bmatrix}, \tag{10d}$$

$$\underline{\underline{\hat{L}}}_{i+1/2} = \begin{bmatrix} \underline{\underline{L}}_i & \underline{\underline{0}} \\ \underline{\underline{0}} & \underline{\underline{L}}_{i+1} \end{bmatrix}. \tag{10e}$$

The domain boundary is handled similarly. In the case of the left boundary, the block is composed of the first two cells. In this case, the retained angular fluxes are the angular fluxes adjacent to the left domain boundary and the two angular fluxes on the cell boundary in the block interior. The angular flux on the right side of cell 2 is discarded. The boundary condition is evaluated at time $k+1$ and the incident angular flux entering the block from cell 3 is evaluated at time k (see Figure 1, *right*). Therefore, the surface flux is defined as

$$\underline{\psi}^{k,surf}_{n,3/2} = \begin{bmatrix} \psi^{b,k+1}_{n,L} \\ \psi^{k+1}_{n,1,R} \\ \psi^{k+1}_{n,2,L} \\ \psi^{k+1/2}_{n,2,R} \end{bmatrix}, \qquad \mu_n > 0\,, \tag{11a}$$

$$\underline{\psi}^{k,surf}_{n,i+1/2} = \begin{bmatrix} \psi^{k+1/2}_{n,1,L} \\ \psi^{k+1}_{n,1,R} \\ \psi^{k+1}_{n,2,L} \\ \psi^{k}_{n,2,R} \end{bmatrix}, \qquad \mu_n < 0\,. \tag{11b}$$

Analogous equations exist for the right boundary. Reflecting boundaries are handled using ghost zones.

2.2. Solving the Staggered-Block Jacobi Equations

To solve the SBJ equations, consider the surface term in Eq. (7). This term can be rearranged as

$$\mu_n \underline{\underline{\hat{L}}}^{surf}_{i+1/2}\underline{\psi}^{k,surf}_{n,i+1/2} = \mu_n \underline{\underline{\hat{P}}}_n \underline{\psi}^{k+1,SBJ}_{n,i+1/2} + \mu_n \underline{\underline{\hat{R}}}_n \underline{\psi}^{k,edge}_{n,i+1/2} \tag{12}$$

where, for $\mu_n > 0$,

$$\underline{\underline{\hat{P}}}_n = \begin{bmatrix} 0 & 0 & 0 & 0 \\ 0 & 1 & 0 & 0 \\ 0 & -1 & 0 & 0 \\ 0 & 0 & 0 & 1 \end{bmatrix}, \tag{13a}$$

$$\underline{\underline{\hat{R}}}_n = \begin{bmatrix} -1 & 0 & 0 & 0 \\ 0 & 0 & 0 & 0 \\ 0 & 0 & 0 & 0 \\ 0 & 0 & 0 & 0 \end{bmatrix}, \tag{13b}$$

$$\underline{\psi}^{k,edge}_{n,i+1/2} = \begin{bmatrix} \psi^k_{n,i-1,R} \\ 0 \\ 0 \\ 0 \end{bmatrix}, \tag{13c}$$

and for $\mu_n < 0$,

$$\underline{\underline{\hat{P}}}_n = \begin{bmatrix} -1 & 0 & 0 & 0 \\ 0 & 0 & 1 & 0 \\ 0 & 0 & -1 & 0 \\ 0 & 0 & 0 & 0 \end{bmatrix}, \tag{14a}$$

$$\underline{\underline{\hat{R}}}_n = \begin{bmatrix} 0 & 0 & 0 & 0 \\ 0 & 0 & 0 & 0 \\ 0 & 0 & 0 & 0 \\ 0 & 0 & 0 & 1 \end{bmatrix}, \tag{14b}$$

$$\underline{\psi}^{k,edge}_{n,i+1/2} = \begin{bmatrix} 0 \\ 0 \\ 0 \\ \psi^k_{n,i+2,L} \end{bmatrix}. \tag{14c}$$

On the left boundary, for $\mu_n > 0$, we have

$$\underline{\psi}^{k,edge}_{n,3/2} = \begin{bmatrix} \psi^{b,k+1}_{n,L} \\ 0 \\ 0 \\ 0 \end{bmatrix}. \tag{15}$$

An analogous boundary flux exists for the right boundary.

Rearranging Eqs. (7), we have

$$\left(\frac{1}{v\Delta t_{k+1}}\underline{\underline{\hat{M}}}_{i+1/2}+\mu_n\underline{\underline{\hat{P}}}_n-\mu_n\underline{\underline{\hat{L}}}_{i+1/2}+\underline{\underline{\hat{T}}}_{i+1/2}\right)\underline{\psi}^{k+1,SBJ}_{n,i+1/2}=\frac{1}{v\Delta t_{k+1}}\underline{\underline{\hat{M}}}_{i+1/2}\underline{\psi}^{k}_{n,i+1/2}$$
$$-\mu_n\underline{\underline{\hat{R}}}_n\underline{\psi}^{k,edge}_{n,i+1/2}+\frac{1}{2}\underline{\underline{\hat{S}}}_{i+1/2}\sum_{m=1}^{N}\underline{\psi}^{k+1,SBJ}_{n,i+1/2}\Delta_m+\underline{\underline{\hat{M}}}_{i+1/2}\underline{Q}^{k+1}_{n,i+1/2}\,. \quad (16)$$

Defining

$$\underline{\underline{\hat{A}}}^{k+1}_{n,i+1/2}=\frac{1}{v\Delta t_{k+1}}\underline{\underline{\hat{M}}}_{i+1/2}+\mu_n\underline{\underline{\hat{P}}}_n-\mu_n\underline{\underline{\hat{L}}}_{i+1/2}+\underline{\underline{\hat{T}}}_{i+1/2}\,, \quad (17)$$

and multiplying through by the inverse of $\underline{\underline{\hat{A}}}^{k+1}_{n,i+1/2}$, we find

$$\underline{\psi}^{k+1,SBJ}_{n,i+1/2}=\frac{1}{v\Delta t_{k+1}}\left(\underline{\underline{\hat{A}}}^{k+1}_{n,i+1/2}\right)^{-1}\underline{\underline{\hat{M}}}_{i+1/2}\underline{\psi}^{k}_{n,i+1/2}-\mu_n\left(\underline{\underline{\hat{A}}}^{k+1}_{n,i+1/2}\right)^{-1}\underline{\underline{\hat{R}}}_n\underline{\psi}^{k,edge}_{n,i+1/2}$$
$$+\frac{1}{2}\left(\underline{\underline{\hat{A}}}^{k+1}_{n,i+1/2}\right)^{-1}\underline{\underline{\hat{S}}}_{i+1/2}\sum_{m=1}^{N}\underline{\psi}^{k+1,SBJ}_{n,i+1/2}\Delta_m+\left(\underline{\underline{\hat{A}}}^{k+1}_{n,i+1/2}\right)^{-1}\underline{\underline{\hat{M}}}_{i+1/2}\underline{Q}^{k+1}_{n,i+1/2}\,. \quad (18)$$

Operating on Eqs. (18) by $\sum_{n=1}^{N}(\cdot)\Delta_n$, we have

$$\left[\underline{\underline{I}}-\frac{1}{2}\left(\sum_{n=1}^{N}\left[\underline{\underline{\hat{A}}}^{k+1}_{n,i+1/2}\right]^{-1}\Delta_n\right)\underline{\underline{\hat{S}}}_{i+1/2}\right]\sum_{n=1}^{N}\underline{\psi}^{k+1,SBJ}_{n,i+1/2}\Delta_n$$
$$=\frac{1}{v\Delta t_{k+1}}\sum_{n=1}^{N}\left(\underline{\underline{\hat{A}}}^{k+1}_{n,i+1/2}\right)^{-1}\underline{\underline{\hat{M}}}_{i+1/2}\underline{\psi}^{k}_{n,i+1/2}\Delta_n-\sum_{n=0}^{N}\mu_n\left(\underline{\underline{\hat{A}}}^{k+1}_{n,i+1/2}\right)^{-1}\underline{\underline{\hat{R}}}_n\underline{\psi}^{k,edge}_{n,i+1/2}\Delta_n$$
$$+\sum_{n=1}^{N}\left(\underline{\underline{\hat{A}}}^{k+1}_{n,i+1/2}\right)^{-1}\underline{\underline{\hat{M}}}_{i+1/2}\underline{Q}^{k+1}_{n,i+1/2}\Delta_n\,. \quad (19)$$

Now our system may be solved using Eqs. (18) and (19).

3. ANALYZING THE STAGGERED-BLOCK JACOBI METHOD

3.1. The Staggered-Block Jacobi Method in the Thick Limit

Let us consider the staggered-block Jacobi method with a homogeneous medium and a uniform mesh. Performing an asymptotic analysis of the staggered-block Jacobi method in the diffusion limit, we find:

$$\frac{\Delta x}{v\Delta t_{k+1}}\left(\phi^{k+1}_{i+1/2}-\phi^{k}_{i+1/2}\right)-\frac{D}{\Delta x}\left(\phi^{k}_{i-1/2}-2\phi^{k+1}_{i+1/2}+\phi^{k}_{i+3/2}\right)$$
$$+\Sigma_a\Delta x\phi^{k+1}_{i+1/2}=\frac{\Delta x}{2}\sum_{n=1}^{N}Q^{k+1}_{n,i,R}\Delta_n+\frac{\Delta x}{2}\sum_{n=1}^{N}Q^{k+1}_{n,i+1,L}\Delta_n\,, \quad (20)$$

where ϕ is the scalar flux, D is the diffusion coefficient, and Σ_a is the absorption cross section. Rearranging this equation, we find

$$\left(\frac{\Delta x}{v\Delta t_{k+1}}+\frac{2D}{\Delta x}+\Sigma_a\Delta x\right)\phi_{i+1/2}^{k+1}=\left(\frac{\Delta x}{v\Delta t_{k+1}}\right)\phi_{i+1/2}^{k} + \left(\frac{D}{\Delta x}\right)\phi_{i-1/2}^{k}+\left(\frac{D}{\Delta x}\right)\phi_{i+3/2}^{k} + \frac{\Delta x}{2}\sum_{n=1}^{N}Q_{n,i,R}^{k+1}\Delta_n+\frac{\Delta x}{2}\sum_{n=1}^{N}Q_{n,i+1,L}^{k+1}\Delta_n\,. \quad (21)$$

From Eq. (20), we see that the scalar fluxes in the diffusion stencil are not all evaluated at the same time step. The consequence of this is that the staggered-block Jacobi method is not conservative. Furthermore, examining Eq. (21), we see that the staggered-block Jacobi method is unconditionally-stable and positive in the thick, diffusive limit. Empirically, we have not yet discovered a problem for which the above staggered-block Jacobi method is not unconditionally stable.

3.2. Restoring Particle Balance

As seen in the previous section, the staggered-block Jacobi method does not preserve particle balance. Particle conservation over the problem domain (rather than *cell-wise* conservation) can be restored using a rebalance procedure, in which the conservative flux $\underline{\psi}_{n,i}^{k+1,cons}$ is calculated using

$$\underline{\psi}_{n,i}^{k+1,cons}=\gamma^{k+1}\underline{\psi}_{n,i}^{k+1,SBJ}\,, \quad (22)$$

where:

$$\gamma^{k+1}=\frac{\text{flux at time } k \text{ + source + particles leaving domain}}{\text{non-conservative flux at } (k+1) \text{ + particles absorbed + incident particles}}\,. \quad (23)$$

It is also possible to use a coarse-mesh rebalance procedure to achieve particle conservation over smaller segments of the problem domain.

3.3. Improving Accuracy using Stretched Sweeps

Because the incident angular flux is lagged to the previous timestep, the SBJ method is accurate when the particle wave moves less than one cell per timestep, i.e., where the problem is thick and diffusive and the wave speed is slow. This is the opposite behavior of mesh sweeps, which are accurate in thin, streaming regions. Therefore, we can improve accuracy by using a sweep at the beginning of each time step. However, accuracy may still be poor in intermediate problems. This can be mitigated by *stretching* the sweep in order to maximize the mean-free path of the streaming particles. Consider the following time-discretized stretched sweep equation:

$$\frac{\epsilon}{v\Delta t_{k+1}}\left(\psi_0^{k+1}-\psi^k\right)+\mu\frac{\mathrm{d}}{\mathrm{d}x}\psi_0^{k+1}+\frac{\Sigma_t}{\epsilon}\psi_0^{k+1}=\frac{1}{2}\left(\frac{\Sigma_t}{\epsilon}-\epsilon\Sigma_a\right)\phi^k+\epsilon Q^{k+1}\,. \quad (24)$$

In the thin-streaming limit, this equation is exact for $\epsilon = 1$. For thick problems, we wish to maximize the mean-free path of the particles. Rearranging Eq. (24), we find

$$\mu \frac{\mathrm{d}}{\mathrm{d}x}\psi_0^{k+1} + \left(\frac{\Sigma_t}{\epsilon} + \frac{\epsilon}{v\Delta t_{k+1}}\right)\psi_0^{k+1} = \frac{1}{2}\left(\frac{\Sigma_t}{\epsilon} - \epsilon\Sigma_a\right)\phi^k + \frac{\epsilon}{v\Delta t_{k+1}}\psi^k + \epsilon Q^{k+1}\,. \tag{25}$$

The $\left(\frac{\Sigma_t}{\epsilon} + \frac{\epsilon}{v\Delta t_{k+1}}\right)$ term represents the inverse of the mean free path. Finding the maximum of this term gives

$$\epsilon = \sqrt{v\Sigma_t\Delta t_{k+1}}\,. \tag{26}$$

Therefore, our stretching parameter is:

$$\epsilon = \begin{cases} 1\,, & \text{thin limit}\,, \\ \sqrt{v\Sigma_t\Delta t}\,, & \text{thick, diffusive limit}\,. \end{cases} \tag{27}$$

Any stretching function used in practice should interpolate between these two limits. There is no unique interpolating function, but the function that we have employed for the numerical results shown in this paper is

$$\epsilon_i^{k+1} = 1.0 + \sqrt{v\Delta t_{k+1}\Sigma_{t,i}}\left[1.0 - e^{-(0.07v\Delta t_{k+1}\Sigma_{t,i})}\right]\,. \tag{28}$$

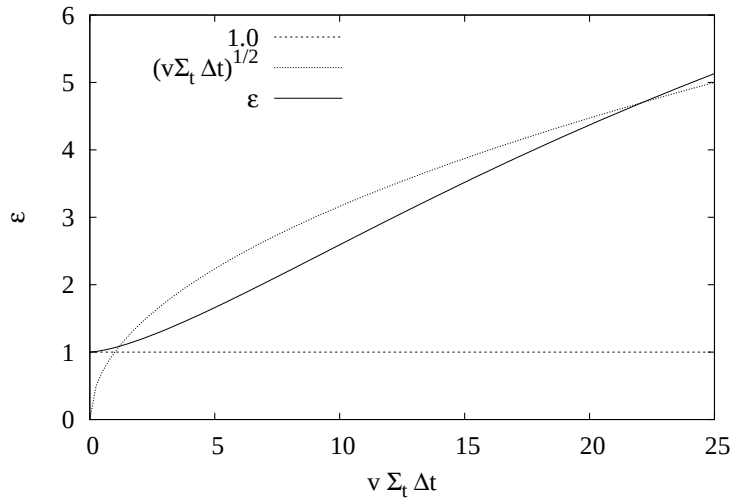

Figure 2. The Interpolating Function ϵ_i^{k+1}

Figure 2 shows a graph of the ϵ parameter in the thick and thin limits, as well as our interpolating function. The graph shows how the interpolating function smoothly interpolates from the thin to thick limits over a range of $0 \leq v\Sigma_t\Delta t \leq 25$. Further research into better interpolating functions may give improved results.

3.4. Iterating the SBJ Method

Finally, we note that the accuracy of the entire scheme can be improved by iterating. If we use the results from the SBJ solution as the lagged incident source on each block to calculate another SBJ solution, we can iterate over the incident fluxes. Iterating to convergence actually gives the same results as the implicit method. However, we have found that more accurate results can be obtained for some problems if we stop iterating before convergence. The algorithm for ceasing the iterations used in the numerical results shown in this paper is:

1. Iterate until relative error < 0.5,
2. If $|\gamma - 1| \leq 0.05$ or relative error < 0.1 cease iterating.

4. NUMERICAL RESULTS

Figures 3, 4 and 5 show numerical results for a planar geometry, one-group, isotropically and purely-scattering problem of width 1.0 cm, divided into 100 cells. We vary Σ_t from 10^{-2} cm^{-1} to 10^6 cm^{-1} and set an internal source of 1.0 in the left-most cell and no internal source elsewhere. We also set the particle speed at $v = 1.0$ cm/s, a reflecting boundary on the left, and a vacuum boundary on the right. The initial condition is zero everywhere, and we use a time step of $\Delta t = 1.0$ sec. We ran a benchmark solution using a time step of $\Delta t = 10^{-5}$ sec. Our final simulation time is $t_f = 1.0$ seconds.

We calculate the L_1 error between the simulation results and the benchmark results using:

$$L_1 \text{ Error} = \frac{\sum_{i=1}^{I} |\phi_i^{\text{Benchmark}} - \phi_i| \Delta x_i}{\sum_{i=1}^{I} \phi_i^{\text{Benchmark}} \Delta x_i}. \tag{29}$$

Figure 3 shows the L_1 errors for the implicit method and plain SBJ with no conservation, sweeps, or iterations. Here we see that, as expected, the SBJ method is accurate as Σ_t becomes large and the particle wave speed becomes slow, but for streaming problems the accuracy is poor. The right side of Figure 4 shows results for SBJ with conservation and a single stretched sweep. Here we see that the sweep has significantly reduced the error in the streaming problems, but the error is still large in intermediate problems. The right side of Figure 5 shows results for SBJ with conservation, a stretched sweep, and iterations using the iteration cessation criteria presented earlier. Here we see that the accuracy of the SBJ method meets or exceeds the accuracy of the standard implicit method. In Figure 6 we show the number of iterations for the SBJ method and the number of iterations for the implicit method (using an Asymptotic-P1 diffusion synthetic acceleration [8] method).

Figure 6 raises an interesting question. Does the SBJ method really require as many iterations as are shown in the figure, or could adequate accuracy be obtained with fewer iterations? Figure 7 shows the L_1 error of the SBJ method with conservation, a stretched sweep, and iterations, but this time the number of iterations is set equal to the number of iterations performed by the implicit method. Here we see that the accuracy of the SBJ method is comparable to that of the implicit

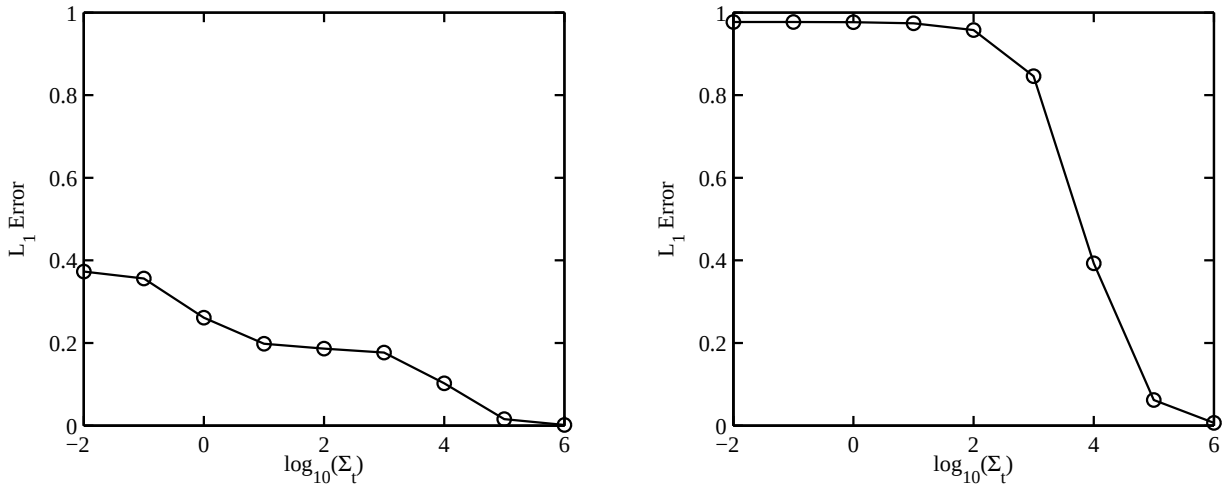

Figure 3. Implicit (*left*) and plain SBJ (*right*)

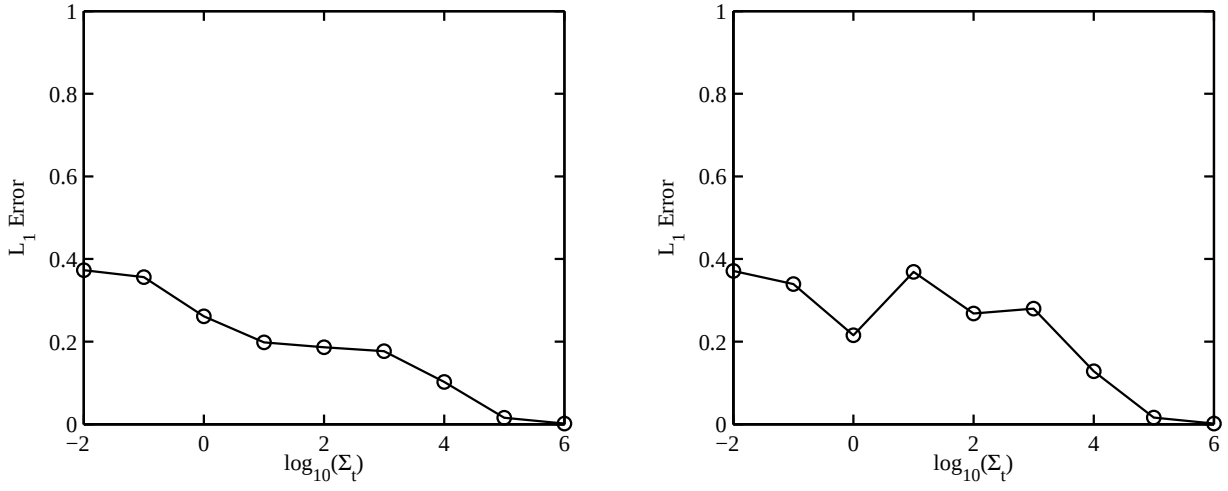

Figure 4. Implicit (*left*) and SBJ with Conservation and a Stretched Sweep (*right*)

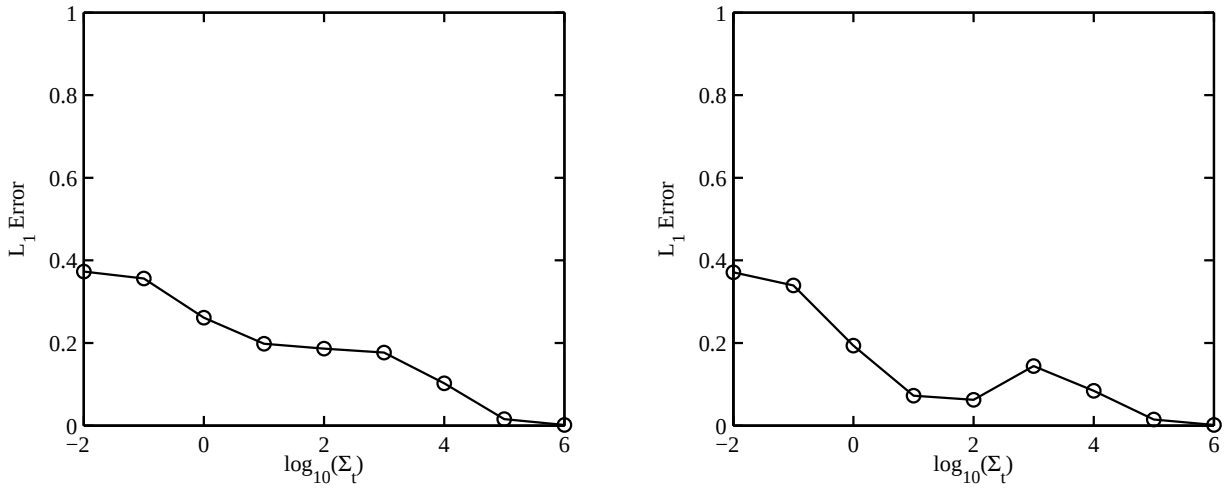

Figure 5. Implicit (*left*) and SBJ with Conservation, a Sweep, and Iterations (*right*)

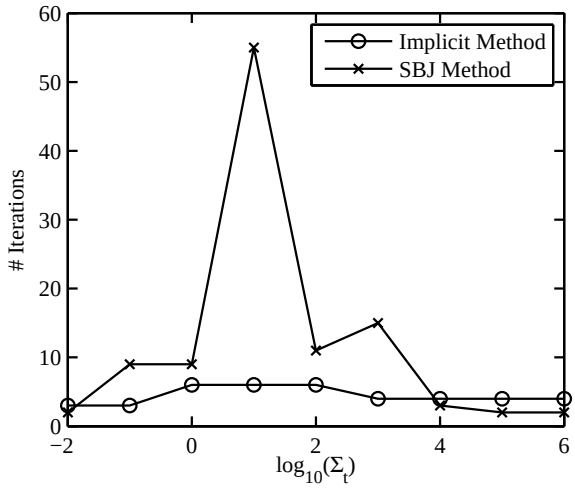

Figure 6. Number of Iterations for the Implicit and SBJ Methods

method even with a small number of iterations. This also implies that further research is needed on iteration cessation algorithms for the SBJ method.

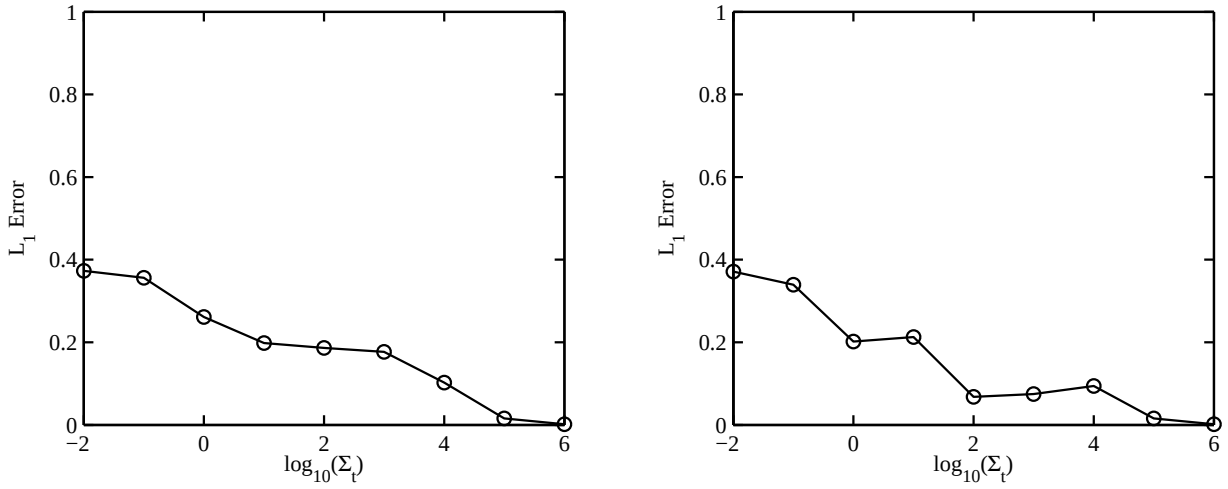

Figure 7. Implicit (*left*) and SBJ with Conservation, a Sweep, and a Few Iterations (*right*)

5. CONCLUSIONS

In summary, the staggered block Jacobi (SBJ) method is a new technique for solving time-dependent transport problems. Traditional deterministic transport methods solve a steady-state transport problem within each time step using mesh sweeps. The SBJ method can solve time-dependent transport problems without sweeps, which makes it easily parallelizable. It is complementary to sweep-based methods in that it is optimal for optically thick media and inefficient for optically thin media. By combining the SBJ method with a stretched sweep and iterations, one can obtain a scheme that is accurate in a variety of regimes.

ACKNOWLEDGEMENTS

This work was performed under a contract from Los Alamos National Laboratory, which is operated by Los Alamos National Security, LLC, for the National Nuclear Security Administration of the U.S. Department of Energy under contract DE-AC52-06NA25396.

REFERENCES

[1] A. Klar, "An Asymptotic-Induced Scheme for Nonstationary Transport Equations in the Diffusive Limit," *SIAM J. Numer. Anal.*, **35**, pp. 1073-1094 (1998).

[2] A. Klar and A. Unterreiter, "Uniform Stability of a Finite Difference Scheme for Transport Equations in Diffusive Regimes," *SIAM J. Numer. Anal.*, **40**, pp. 891-913 (2002).

[3] G. Davidson and E.W. Larsen, "An Unconditionally-Stable Time-Dependent Transport Method Without Sweeps," *Trans. Am. Nucl. Soc.*, **97**, pp. 530-532 (2007).

[4] M.L. Adams, "Discontinuous Finite Element Transport Solutions in Thick Diffusive Problems," *Nucl. Sci. Eng.*, **137**, pp. 298-333 (2001).

[5] E. E. Lewis and W.F. Miller, Jr., *Computational Methods of Neutron Transport*, American Nuclear Society, La Grange Park, Il., USA (1993).

[6] M.L. Adams and E.W. Larsen, "Fast Iterative Methods for Discrete-Ordinates Particle Transport Calculations," *Progress in Nuclear Energy*, **40**, No. 1, 3-159 (2002).

[7] B.W. Patton and J.P. Holloway, "Application of Krylov Subspace Iterative Methods to the Slab Geometry Transport Equation," *Proc. ANS Topical Meeting, Advancements and Applications in Radiation Protection and Shielding*, Cape Cod, April 21-25, 1996, Vol. 1, p. 384 (1996).

[8] T.A. Wareing, "Asymptotic Diffusion Accelerated Discontinuous Finite Element Methods for Transport Problems," Ph.D. Dissertation, University of Michigan (1991).